EPJ D
Atomic, Molecular, Optical and Plasma Physics
EPJ.org
your physics journal

Eur. Phys. J. D **59**, 133–137 (2010) DOI: 10.1140/epjd/e2010-00091-x

Boundary-induced localized structures in a nonlinear optical feedback experiment

M. Ayoub, F. Papoff, G.L. Oppo and C. Denz

EDP SCIENCES
Società Italiana di Fisica
Springer

Eur. Phys. J. D **59**, 133–137 (2010)
DOI: 10.1140/epjd/e2010-00091-x

THE EUROPEAN PHYSICAL JOURNAL D

Regular Article

Boundary-induced localized structures in a nonlinear optical feedback experiment

M. Ayoub[1,a], F. Papoff[2], G.L. Oppo[2], and C. Denz[1]

[1] Institute of Applied Physics and Center for Nonlinear Science, Westfälische Wilhelms-Universität Münster, Corrensstr. 2/4, 48149 Münster, Germany
[2] Institute of Complex Systems, SUPA and Department of Physics, University of Strathclyde, 107 Rottenrow, Glasgow G4 0NG, Scotland, UK

Received 6 January 2010
Published online 6 April 2010 –

Abstract. Experimental and numerical evidence of symmetry-breaking bifurcations of a circular dissipative soliton with additional boundary conditions in the feedback of a liquid crystal light valve are reported. By tuning the strength of the nonlinearity or the size of the additional boundaries, the circular structure breaks up into polygonal symmetries and the system exhibits multistability. The experimental results are confirmed by numerical simulations with different configurations of the polarizers thus demonstrating the universality of the phenomenon.

1 Introduction

The existence of dissipative localized structures in optical cavities, also known as cavity solitons, is well-known for many nonlinear photonic devices driven far from an equilibrium state [1]. Dissipative solitons are static or dynamical localized objects that experience gain and loss of their energy during the propagation. They can form where the overall gain, loss and diffraction are balanced [1,2]. In optical systems they have been observed in active and passive optical cavities, but also in single mirror feedback experiments with different optical nonlinearities [1,3–6]. Formation of dissipative localized structures is combined, in general, with an organized nonlinear behavior such as optical bistability. Due to bistability, dissipative solitons have binary features and a robust spatial shape based on the balance of diffraction and nonlinearity, allowing one to control and guide them easily in intensity and phase gradients [7–10]. This latter fact can be attractive for applications in the context of all optical information processing where solitary structures are used as 'optical bits' [3,7]. Systems based on liquid crystal light valves (LCLV) display a rich set of different spatial structures such as regular patterns (hexagons, negative hexagons, rolls), spatiotemporal chaos, and localized structures [11,12]. Spatially localized structures in LCLV mainly exist in the range of optical bistability [11] and can have circular or other reduced symmetries. Different symmetries may coexist in the same system, due to the breaking of the rotational symmetry for certain ranges of control parameters. In these cases, triangular symmetry of localized states has been observed [13] and accompanied by the appearance of phase singularities [14]. Here we investigate, both experimentally and numerically, the breaking of the circular symmetry of localized states with the aim of explaining bifurcations to symmetries that are more complex than the triangular one when imposing boundary limitations and choosing a suitable control parameter range. These novel localized states with peculiar symmetries may be used as multi-state pixels in nonlinear optical information processing and allow a considerable increase in storage capacity of 'optical bits' with respect to the standard localized state of circular symmetry.

2 Experimental set-up and theoretical model

Experimentally, the Kerr medium used is a reflective LCLV used as a hybrid nonlinear element placed in a feedback loop. LCLV, in spite of the relatively slow response time estimated in the range of 50 ms, are attractive as nonlinear elements in this type of experiments due to the high nonlinear sensitivity and the large aspect ratio. This enables the observation of patterns of broad area and the choice of one of several spatially periodic structures when using Fourier filtering [15].

The LCLV device works as an optically addressable spatial light modulator as a function of the writing intensity and the external applied voltage. The LCLV is constructed of a set of thin layers, which are two transparent indium tin dioxide-coated glass electrodes, a liquid crystal layer (LC), a dielectric mirror, a sensitive absorber, and a photoconducting layer. The LCLV can be divided into

[a] e-mail: ayoubm@uni-muenster.de

two functional sides: a read and a write side. The principle function of LCLV is the conversion of a spatial light intensity distribution incident on the photoconduction layer in a modulation of the refractive index of the liquid crystal layer. A read wave passes the (LC) layer, is reflected at the dielectric mirror, and leaves the LCLV modulated in its phase and polarization state. The phase shift Φ of the extraordinary wave induced by the LCLV can be written as [11,16]:

$$\tau\frac{\partial}{\partial t}\Phi - l^2\nabla_\perp^2\Phi + \Phi = \Phi_{max}\left\{1-\tanh^2\left(\frac{V_{lc}-V_{th}}{V_0}\right)\right\} = \Phi_{max}\left\{1-\tanh^2\left(\mu I_w + \Phi_0\right)\right\}, \quad (1)$$

where $\Phi_{max} = 2k\Delta n$ is the maximum phase shift, Δn is the difference between the extraordinary and ordinary refractive indices, τ denotes the effective response time of the liquid crystals required for their reorientation, $\nabla_\perp^2$ is the Laplacian operator, and l is the effective diffusion length accounting for the restricted spatial resolution of the LCLV. V_{th} and V_{lc} are respectively the threshold voltage and the voltage drop of the liquid crystal layer, here normalized to V_0. I_w is the intensity distribution on the write side of the LCLV while μ and Φ_0 are related to the sensitivity and bias of the LC voltages on I_w. Model (1) contains the temporal and spatial resolutions and the effects of saturation, in short, it describes the response of the material. After illuminating the LCLV with a certain polarized light, the illuminating field is modulated in phase and its polarization is changed. A polarizer has been used in our experiments to transfer the phase modulation into an amplitude modulation. The resulting intensity distribution I_w at the write side after free propagation over a distance L can be written as:

$$I_w = \left|\exp\left(\frac{-iL}{2k_\lambda}\nabla_\perp^2\right)(Be^{-ik\Phi}) + C\right|^2 I_p, \quad (2)$$

where k_λ and k denote the wave numbers of the light field and of the macroscopic spatial modulation over the instability threshold respectively, I_p is the LCLV input intensity, and the amplitude factors B and C are given by $B = \cos\psi_1\cos\psi_2$ and $C = \sin\psi_1\sin\psi_2$; ψ_1 and ψ_2 are the angle of the input polarization and the angle of the polarizer axis respectively, regarding to the optical axis of the liquid crystal layer. If $\psi_1 = \psi_2 = 0$, which means $B = 1$ and $C = 0$, pure phase modulations are induced in the system. The LCLV system of Figure 1 is well described by the two equations (1), (2). The experiments presented here have been performed with different arrangements of polarizers, $\psi_1 \neq \psi_2 \neq 0$. In a polarization mode, a rich diversity of optical patterns has been reported [11,12,17,18]. The reason for this diversity is the additional amplitude modulation induced by the modulation of the polarization state.

A typical experimental setup is shown in Figure 1. The LCLV is driven by a frequency doubled Nd:YAG laser ($\lambda = 532$ nm, $P = 100$ mW). The input I_p is linearly polarized and expanded to a diameter of 3.5 cm. This uniform wave passes the read-out side of LCLV where it is internally reflected at the dielectric mirror and modulated in its phase and polarization state. The modulated wave is then inserted into the feedback loop where the wave passes the polarizer (P2) that transmits the polarization direction ψ_2 with respect to the optical axis of the LCLV. After a chosen distance of free space propagation L, the resulting intensity distribution I_w is reflected at mirrors M, goes through the lenses L, to reach the write side of the LCLV, thus closing the feedback loop. In the following section, we present results of imposing transverse boundary limitations to the feedback loop on selected solitary structures.

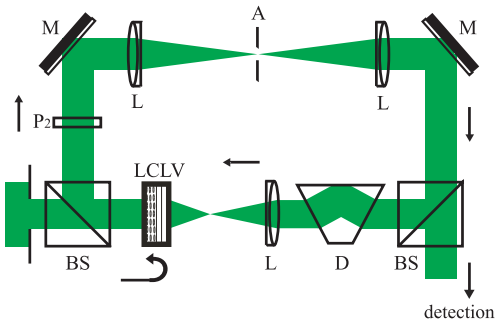

Fig. 1. (Color online) Experimental setup of the LCLV single feedback experiment system. P2: polarizer determining ψ_2, L: lenses, M: mirrors, BS: beam splitter, D: dove prism.

3 Boundary-induced localized structures in LCLV

The influence of boundaries on regular patterns has already been studied theoretically and experimentally in active and passive nonlinear media [19–22]. In this work, we consider experimentally and numerically how boundaries affect solitary structures by applying circular apertures in a range of parameters different from those investigated previously [13].

Solitary structures are observed in polarization modulation with different polarizer configurations. The case $\psi_1 = \psi_2$ was investigated in [13,18] while we work here mainly with $\psi_1 = -\psi_2$. In our experiment we use angles of $\psi = 44°$, a free propagation length of $L = -20$ cm, a LC voltage of 4.4 V, and a frequency of 250 Hz. With these parameters, solitary structures begin to appear at $I_w \approx 0.12$ mW/cm^2 above the instability threshold. When increasing the input intensity, more solitary structures arise and coexist in the transverse plane of the wave. At higher intensity values, they form a collection of uncorrelated solitary structures. These collections are constituted by moving spots and do not display spatial order.

To apply additional spatial boundaries, an aperture is placed in front of the write side of the LCLV after the solitary structures are formed. The total diameter of the impinging feedback beam on the write side of the LCLV is 2.3 cm, whereas the diameter of the aperture varies from

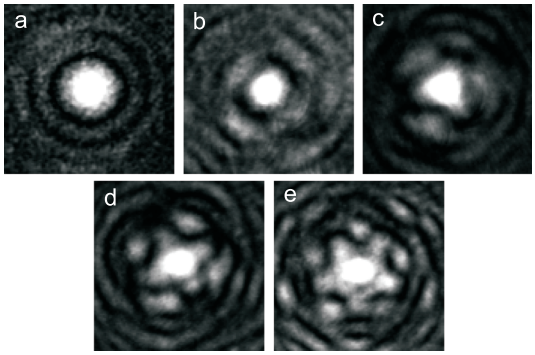

Fig. 2. Different symmetries of spatial solitary structures observed at fixed input power and at the aperture sizes: (a) 0.9 mm, (b) 0.98 mm, (c) 1.17 mm, (d) 1.19, (e) 1.2 mm. The structures differ from each other in size, symmetry and in the number of the radial oscillations.

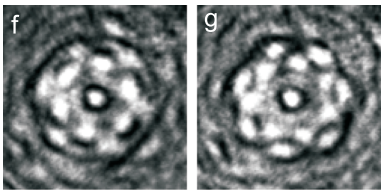

Fig. 3. Hexagonal and heptagonal structures appearing when further enlarging the aperture to (f) 1.34 mm, (g) 1.4 mm and for higher nonlinearity than in Figure 2.

0.08 to 2 cm. Starting from the aperture diameter 0.9 mm where only a single solitary structure is allowed to pass the aperture, and increasing it slightly, the strong nonlinearity modifies the original circular symmetry in order to fit the aperture area. The sequence of observed structures with increasing apertures but at a fixed input intensity are shown in Figure 2.

The typical circular localized structure breaks up and loses its highest symmetry when enlarging the aperture from 0.90 mm to 0.98 mm where a novel structure with rectangular symmetry emerges. By further increasing the aperture to 1.2 mm, the structure modifies again and three tails arise. The three tails are arranged symmetrically around the central spot forming a triangular structure similar to the triangular solitons reported in [13]. After the triangular structure, other polygonal symmetries arise when further enlarging the aperture, namely quadratic and pentagonal structures. The central spot has a symmetry corresponding to the number of emerging tails. By further enlarging the aperture, the pentagonal symmetry is destroyed and no clear symmetry is observed. Other symmetries can be observed if the strength of the nonlinearity is large enough to force more structures to fit into the aperture. Experimentally, hexagonal and heptagonal symmetries have been obtained when slightly tuning the nonlinearity by changing the frequency of the applied voltage to 290 Hz, see Figure 3. It is worth noting that the number of tails in the boundary-induced structure is controlled by the aperture size, the LC voltage, the input intensity and the saturation threshold.

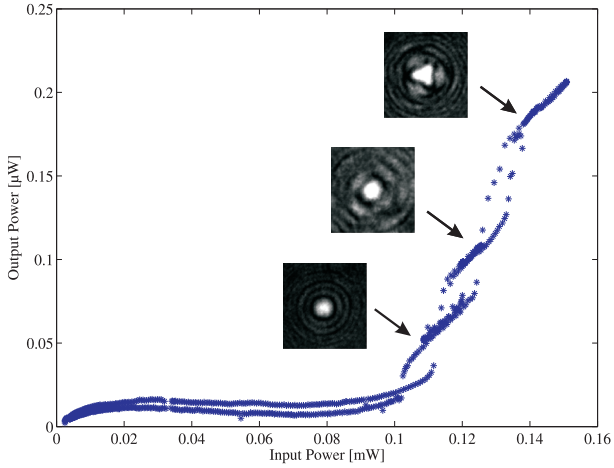

Fig. 4. (Color online) Experimental bistability curve corresponding to the first three symmetries, the circular, rectangular, and triangular one, in the presence of an aperture of size 1.2 mm in the optical feedback path in the polarization mode $\psi_1 = -\psi_2 = 44^\circ$ of the LCLV system.

This experiment demonstrated the transition from *bulk induced* symmetries, where the aspect ratio is large and the emerging structures are independent of the size of the feedback beam, namely the circular and triangular solitary structures, to *boundary induced* symmetries which depend on the size of the aspect ratio and the nonlinearity. We have then investigated the effect of the input intensity on the behavior of the system in the regime of strong dependence from the boundary conditions. As indicated above, the appearance of lower polygonal symmetries is ruled not only by the size of the imposed aperture, but also by the input intensity. The experimental observations indicate that, if the aperture is kept fixed at 1.2 mm, only the rectangular and triangular symmetries can be observed even at high values of the input intensity. The state diagram for this case is shown in Figure 4.

As one sees in Figure 4, the transitions between the observed symmetries when increasing the input intensity are associated with the appearance of boundary-induced bistability regions. If the input intensity is increased, the uniform dark background loses its stability at a certain turning point and the solution switches to a second stable branch of higher output intensity. By further increasing the input intensity, the system loses its stability again and switches to a stable third branch of even higher output intensity. On the other hand, if starting from the third steady state and decreasing the input intensity, the system remains stable until a new turning point before it jumps back to the lower stable branch and so on. The separation of the bistable branches depends also on the polarization configuration. When $\psi_1 = -\psi_2 = 45^\circ$, a maximum separation of the bistability branches representing the steady solutions of the system is obtained.

In comparison with the bistable behavior observed between the circular solitary structure and the triangular one in [13], we observe that the presence of the aperture

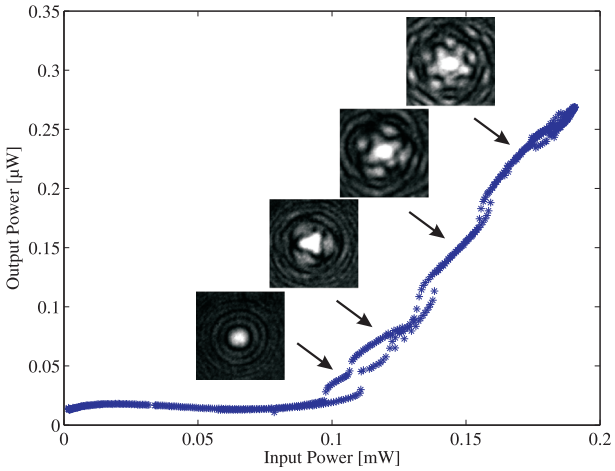

Fig. 5. (Color online) Experimental bistability curve corresponding to the circular, triangular, square and pentagonal symmetries in the presence of an aperture of size 1.4 mm in the optical feedback path in the polarization mode $\psi_1 = -\psi_2 = 44°$ of the LCLV system.

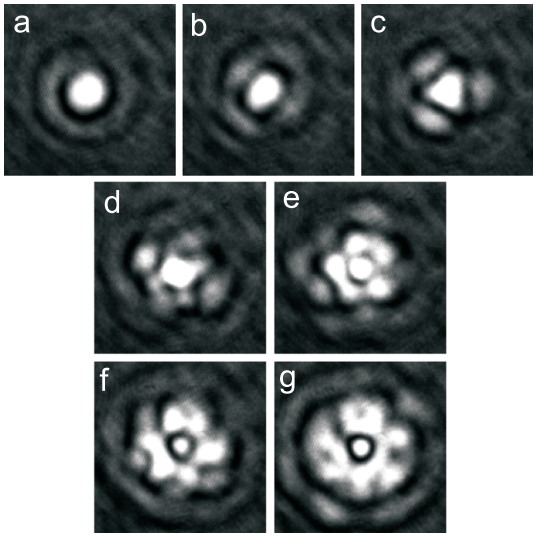

Fig. 6. Experimental spatial solitary structures observed in the LCLV system for $\psi_1 = \psi_2 = 53°$ and an aperture enlarging from 0.8 to 2.5 mm.

leads to the generation of an additional steady state corresponding to the intermediate rectangular structure.

Until now we have considered an aperture with diameter of 1.2 mm. To get a complete picture of the ability of the system to support symmetries different from the circular one, the aperture is increased to ≈1.4 mm, i.e. large enough to allow a pentagonal structure to be observed. The measurements show that at this size of the aperture, the rectangular structure vanishes, and the state diagram depicted in Figure 5 shows four small bistability regions representing four steady states, with a small fifth hysteresis loop corresponding to an unstable hexagonal structure. The hexagonal structure can be stabilized by tuning the applied frequency, i.e. the nonlinearity. Similar multistable behaviors have been described in the numerical simulations of the LCLV system [11].

We note that we have observed a similar set of boundary-induced solitary structures also in the configuration of polarizers $\psi_1 = \psi_2$, as shown in Figure 6. The boundary-induced scenario of bifurcations to polygonal localized states is quite general and should be observable in experiments with optical nonlinearities different from that of the LCLV.

4 Numerical simulations

Numerical simulations of equations (1), (2) have been performed with a split-step method on 256×256 point grids. The free space propagation of the feedback field is computed by multiplying its Fourier transform by the appropriate phase function and then performing the inverse Fourier transform. To reproduce the experiments, an infinitely absorbing screen with a circular aperture is inserted into the feedback loop so that the diameter and position of the writing beam can be controlled. The position of the aperture is always chosen to be at the grid center.

For the case $\psi_1 = -\psi_2$, dissipative solitons have been found at $\psi_1 = 39°$, $40°$, $41°$ and $L = -18$ cm using the model (1)–(2). As in the experiment, we progressively increase the size of the aperture measured in units of the size of the circular soliton observed without aperture. Figure 7 shows localized structures with rectangular, triangular, quadratic, pentagonal, hexagonal, and heptagonal symmetries observed for apertures of diameters of 1.15, 1.25, 1.82, 2.40, 2.77 and 2.92 times the original circular soliton, respectively and $\psi_1 = 41°$.

We have also obtained localized structures with polygonal symmetries when changing the size of the aperture in the case $\psi_1 = \psi_2$. LCLV experiments in this conditions have been performed in [13,18]. Figure 8 shows the sequence of symmetries observed for increasing apertures. Enlarging the aperture diameter to 1.11, the rotational symmetry breaks up yielding a rectangular structure (Fig. 8b) that, in turn, becomes unstable and gives rise to a triangular structure at 1.15 (Fig. 8c). After the triangular ones, structures with quadratic, pentagonal and hexagonal symmetries are observed for aperture diameters of 1.56, 1.94 and 2.0, respectively (Figs. 8d–8f). These observations clearly demonstrate the universal nature of the phenomenon of aperture-induced polygonal symmetries described in the previous sections.

5 Conclusion

We have observed both experimentally and numerically solitary structures with polygonal symmetries ranging from rectangular to heptagonal in a LCLV system with different polarizer configurations $\psi_1 = -\psi_2$ and $\psi_1 = \psi_2$. Most of these symmetries are boundary induced and are not observed for the same values of the control parameters in the same system without a confining aperture. This shows that an aperture can induce boundary effects

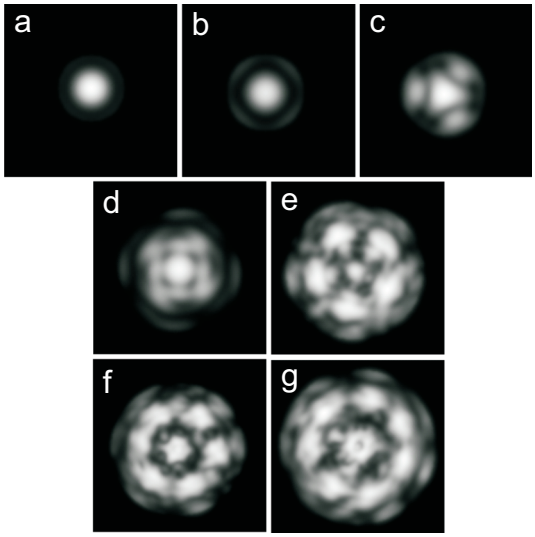

Fig. 7. Numerical simulations of solitary structures for the case of $\psi_1 = -\psi_2 = 41^\circ$ when enlarging the aperture to diameters: (a) 1.0, (b) 1.15, (c) 1.25, (d) 1.82, (e) 2.40, (f) 2.77, and (g) 2.92 times the original circular soliton size.

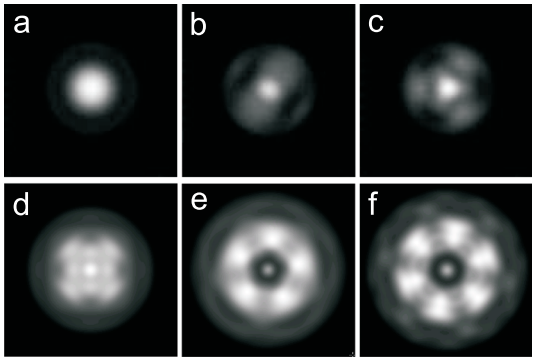

Fig. 8. Numerical simulations of solitary structures for the case of $\psi_1 = \psi_2 = 55^\circ$ and at $\mu I_p = 4$ and $\Phi_0 = 3\pi$ when enlarging the aperture to diameters: (a) 1.0, (b) 1.11, (c) 1.15, (d) 1.56, (e) 1.94, and (f) 2.00 times the original circular soliton size.

strong enough to affect deeply the type and the stability of the observed localized spatial structures. Bistability of the polygonal structures while changing the input power up and down show that the boundary-induced localized structures maintain the nonlinear character of the original circularly symmetric soliton. Our results together with the simplicity of the experimental set-up indicate that apertures can be a very effective way to control bifurcations and instabilities in transverse nonlinear optics.

We thank W.J. Firth for useful discussions. This work is financially supported by DAAD the German Academic Exchange Service and the national academy of science of the UK. G.-L.O. thanks the European Commission for financial support through the HIDEAS collaborations.

References

1. T. Ackemann, W.J. Firth, G.-L. Oppo, Adv. At. Mol. Opt. Phys. **57**, 323 (2009)
2. N. Akhmediev, A. Ankiewics, *Dissipative Solitons* (Springer, 2005)
3. W.J. Firth, C.O. Weiss, Opt. Photonics News **13**, 54 (2002)
4. S. Barland et al., Nature **419**, 699 (2002)
5. B. Schäpers et al., Phys. Rev. Lett. **85**, 748 (2000)
6. A. Schreiber, B. Thüring, M. Kreuzer, Opt. Commun. **136**, 415 (1997)
7. W.J. Firth, A.J. Scroggie, Phys. Rev. Lett. **76**, 1623 (1996)
8. A.J. Scroggie, J. Jeffers, G. McCartney, G.-L. Oppo, Phys. Rev. E **71**, 046602 (2005)
9. U. Bortolozzo, S. Residori, Phys. Rev. Lett. **96**, 037801 (2006)
10. C. Cleff, B. Gütlich, C. Denz, Phys. Rev. Lett. **100**, 233902 (2008)
11. R. Neubecker, G.-L. Oppo, B. Thuering, T. Tschudi, Phys. Rev. A **52**, 791 (1995)
12. S. Residori, Phys. Rep. **416**, 201 (2005)
13. U. Bortolozzo, L. Pastur, P.L. Ramazza, M. Tlidi, G. Kozyreff, Phys. Rev. Lett. **93**, 253901 (2004)
14. P.L. Ramazza, U. Bortolozzo, L. Pastur, J. Opt. A **6**, S266 (2005)
15. G.K. Harkness, G.-L. Oppo, E. Benker, M. Kreuzer, R. Neubecker, T. Tschudi, J. Opt. B **1**, 177 (1999)
16. K. Lu, B.E.A. Saleh, Appl. Opt. **30**, 2354 (1991)
17. B. Thüring, R. Neubecker, M. Kreuzer, E. Benkler, T. Tschudi, Asian J. Phys. **7**, 453 (1998)
18. P.L. Ramazza, S. Ducci, S. Boccaletti, F.T. Arecchi, J. Opt. B: Quantum Semiclass. Opt. **2**, 399 (2000)
19. F. Papoff, G. D'Alessandro, G.-L. Oppo, W.J. Firth, Phys. Rev. A **48**, 634 (1993)
20. E. Pampaloni, P.L. Ramazza, S. Residori, F.T. Arecchi, Europhys. Lett. **25**, 587 (1994)
21. F. Papoff, G. D'Alessandro, G.-L. Oppo, Phys. Rev. A **60**, 648 (1999)
22. F. Papoff, G. D'Alessandro, G.-L. Oppo, W.J. Firth, Phys. Rev. Lett. **82**, 2087 (1999)
23. E. Louvergneaux, D. Hennequin, D. Dangoisse, P. Glorieux, Phys. Rev. A **53**, 4435 (1996)
24. G. D'Alessandro, F. Papoff, E. Louvergneaux, P. Glorieux, Phys. Rev. E **69**, 066212 (2004)